RSC Advances

ROYAL SOCIETY OF CHEMISTRY

www.rsc.org/advances

Decolorization of Acid Orange II dye by peroxymonosulfate activated with magnetic Fe_3O_4@C/Co nanocomposites

Zhijun Xu[a], Jiahua Lu[a] , Qing Liu[a], Lian Duan[b], Aihua Xu[b], Qiang Wang [a,b,*] and Yuguang Li [a,b,*]

[a] School of Chemistry and Chemical Engineering, Wuhan Textile University, Wuhan 430073, China

[b] Engineering Research Centre for Cleaner Production of Textile Printing and Dyeing, Ministry of Education, Wuhan 430073, China

∗ Corresponding author. Tel.: +86(0)27 59367334; Fax: +86(0)27 59367343

E-mail address: wangqche@hotmail.com; qiang_wang@wtu.edu.cn (Q.Wang); liyg2010@wtu.edu.cn (Y. Li)

Abstract:

New metallic cobalt loaded magnetic nanocomposites (Fe_3O_4@C/Co) were prepared by calcination and in-situ reduction of the Co^{2+}–impregnated magnetic carbon nanoparticles of Fe_3O_4@C at 900°C under nitrogen atmosphere. Fourier transform infrared spectroscopy (FT-IR), powder X-ray diffraction (XRD), vibrating sample magnetometer, transmission electron microscopy (TEM) and X-ray photoelectron spectroscopy (XPS) were employed to characterize the properties of the composites and the loading of metallic Co^0 in the material was clarified. The catalytic properties of the nanocomposites Fe_3O_4@C/Co in activating peroxymonosulfate (PMS) for decolorization of Acid Orange II (AO II) dye in aqueous solution were investigated. Fe_3O_4@C/Co nanocomposites exhibited high activity in PMS activation for AO II decolorization. Complete decolorization of AO II solution could be achieved in 20 min within near neutral pH range (pH 6.4-8.5), while a complete decolorization occurred in 40 min for the as-prepared solution without pH adjustment (pH 4.05). The effect of several parameters including pH, catalyst load, PMS concentration and reaction temperature on the catalytic activity were also investigated. Sulfate free radicals activated from PMS were proposed to be the dominant active species in the "Fe_3O_4@C/Co + PMS" system for AO II decolorization. The catalytic and decolorization mechanism was suggested. The catalyst Fe_3O_4@C/Co could be recycled easily by a magnet with good reusability. This study provides a promising way for the activation of "green" oxidant, PMS, by the new magnetic nanocomposites for environmental remediation and oxidation catalysis.

Key words: Dye decolorization; Acid orange II; Peroxymonosulfate; Magnetic separation; Cobalt; Fe_3O_4/C

1. Introduction

Synthetic dyes are among the main organic pollutants and they present in wastewater streams from many industrial sectors including textile, leather, cosmetics, paper, electronics, plastic, pharmaceutical, food and other chemical usages.[1, 2] Among all the synthetic dyes, azo dyes occupy the largest and most important position of dyes for industrial applications, while an estimated 10–15% of the total world production of dyes is lost during the dyeing process and is released in the textile effluents.[3-5] The release of azo dyes into the environment would be harmful to aquatic life and human health because of their toxic, mutagenic and carcinogenic characteristics.[1, 5] Therefore, the degradation and decolorization of wastewater contaminated with azo dyes have aroused worldwide interest.[5, 6] Unfortunately, due to their biological resistance and chemical stability, azo dyes pollutants can hardly be treated using classical wastewater treatment technologies.[7] Therefore, more powerful wastewater treatment methods are highly demanded. Advanced oxidation processes (AOPs) have been used in recent decades as an effective treatment option for the removal of emerging recalcitrant organic contaminants.[8, 9] The AOPs are based on highly reactive species such as hydroxyl (HO•) and/or sulfate (SO_4^{-}•) radicals. These radicals are capable of degrading the organic molecules and yielding intermediates and CO_2. Radical species can be produced mainly from the thermal, UV and transition metal activation of oxidants such as hydrogen peroxide, persulfate (PS) and peroxymonosulfate (PMS).[10-12] As one of the popular AOPs, Fenton reaction using HO• radicals activated from H_2O_2 is able to efficiently decompose various organic contaminants, but it suffers from some demerits such as low pH range (2 – 4) and large amount of sludge produced.[13] Compared with HO• radicals (1.8 – 2.7V), SO_4^{-}• possesses a higher redox potential (2.5–3.1V) with a longer life time and exhibits a higher degradation efficiency for most organic pollutants over a wide pH range ($4 < pH < 9$). PMS also has a higher oxidizing potential (1.82V) than H_2O_2 (1.76 V), and it intervenes in degradation processes in a more efficient way than PS does.[4] PMS has been widely used in oxidative degradation of organic pollutants due to its higher stability and ease of storage, transport and handling compared to H_2O_2.[14, 15] PMS is a triple salt of potassium monopersulfate ($2KHSO_5$•$KHSO_4$•K_2SO_4), a product manufactured by DuPont, and commercially available as OXONE®. PMS is considered to be a green oxidant because it is benign, as are most of the byproducts of its reactions. The decomposition rate of organic compounds with PMS at room temperature is low, but it can be enhanced through activation by photolysis or thermolysis (Eq.(1)) or by

using transition metals such as manganese, iron and cobalt (Eq. (2)), thereby producing highly reactive SO_4^{-}• and HO• radicals.[4, 10]

$$HSO_5^- \xrightarrow{h\upsilon/\Delta} SO_4^{-}\bullet + HO\bullet \quad (1)$$

$$HSO_5^- + \text{Metal ion } (M^{n+}) \rightarrow M^{n+1} + SO_4^{-}\bullet + OH^- \quad (2)$$

Homogeneous reactions using cobalt ions to activate PMS were proven of high efficiency for oxidation of organic compounds.[16] However, the loss of cobalt from the homogeneous processes leads to metal pollution, which may cause several health problems.[10, 17] Heterogeneous activation of peroxymonosulfate would provide a good solution and many efforts have been carried out for developing heterogeneous oxidation systems with high activity. For example, several investigations have been reported in using cobalt oxides,[18, 19] supported cobalt compounds,[8, 20] and Co-exchanged zeolites,[21] etc as heterogeneous catalysts for activation of PMS. Many materials, such as metal oxide, silica, carbon, zeolite, polymer resins, and nanocomposites, have been developed as catalyst support for preparing heterogeneous catalyst. Compared to polymer and silica shells, carbon shells exhibit much higher stability in rigorously environments including acid or base media, as well as at high temperatures and pressures.[22] Moreover, hydrophilic groups can be generated on the surface of carbon shell, making hybrid nanoparticles being negatively charged to further enhance their colloidal stability and biocompatibility and load other metal nanoparticles on their surfaces.[23] Therefore, carbon materials have been regarded as promising candidates of supporter for heterogeneous catalyst.[20, 24, 25] On the other hand, magnetic Fe_3O_4 loaded materials have numerous advantages such as high separation efficiency, simple manipulation process, and easy operation conditions. Magnetic separation can remove nanoparticles in water simply by using an external magnetic field, indicating great potentials for practical applications in wastewater treatment technology.[13, 26] Core/shell magnetic carbon nanospheres have recently attracted intense attention owing to their unique magnetic response, low cytotoxicity and highly functionable surface.[13, 22] For example, Wang *et al* prepared magnetic Mn catalysts using Fe_3O_4 as the magnetic core, carbon spheres as barrier and manganese oxide nanoparticles as functional component. These magnetically separable catalysts demonstrated to be effective for activation of PMS in producing oxidative radicals for phenol degradation.[13] Magnetic carbon core/shell nanospheres were also employed by Wang *et al* to load Co_3O_4 by an impregnation method, and the prepared magnetic carbon sphere supported Co_3O_4 composites exhibited high activity in PSM activation for

phenol degradation with 100% conversion within 30 min.[8] Metal nanoparticles are highly attractive in catalytic reactions. Li *et al* prepared multifunctional Ag-loaded Fe_3O_4@C by loading Ag nanocrystals onto the surface carbon shell of Fe_3O_4@C nanospheres. The synthesized Ag-Fe_3O_4@C nanocomposite exhibited excellent catalytic activity toward organic dye with 98% of RhB conversion within 20 min in the presence of $NaBH_4$.[22] Gong *et al* reported the synthesis of magnetic core/shell Co@C spheres via a one-pot approach through catalytic carbonization of mixed PP/PE/PS by Co_3O_4. The core/shell Co@C spheres showed high performance in the photo-degradation of Congo Red (CR). It was demonstrated that the outer carbon shell promoted the degradation of CR and served as a protective layer for cobalt core to improve acid resistance, while the inner cobalt core accelerated the decomposition of H_2O_2 into radicals, which catalyzed the degradation of CR.[25] It is of note that the copper nanoparticles loaded Fe_3O_4@C/Cu magnetic core/shell microspheres exhibit much higher photocatalytic activity for degradation of methylene blue (MB) in comparison with Fe_3O_4@CuO under visible light irradiation and in the presence of H_2O_2. It was proposed that the Cu nanocrystals can exhibit the collective oscillation of the conduction electrons upon interaction with electromagnetic radiation, which can effectively promote visible light absorption.[27] Yao *et al* recently reported the preparation of Co-graphene hybrids with metal cobalt nanoparticles anchored on graphene nanosheets and the hybrids exhibit high catalytic activity in the degradation of orange II.[28] However, the reports of Fe_3O_4@C/metal magnetic nanocomposites for catalytic removal of organic pollutants using PMS are still very limited. To the best of our knowledge, no investigation on metallic cobalt loaded Fe_3O_4@C magnetic nanocomposites catalyst, namely Fe_3O_4@C/Co, for PMS activation has been yet reported for the decolorization of organic dyes solution.

We report herein the preparation of a new nanocomposite of magnetic carbon nanospheres supported cobalt, Fe_3O_4@C/Co, via the approach as described in Scheme 1. The magnetic nanocomposite, Fe_3O_4/C, was first prepared by an ultrasonic irradiation-hydrothermal method. And the cobalt is supported onto Fe_3O_4/C by impregnation method followed by in-situ reduction with heat treatment under nitrogen atmosphere. The Fe_3O_4@C/Co catalyst was characterized and its catalytic performances and magnetic separation/reusability were investigated for the decolorization of Acid Orange II solution with peroxymonosulfate.

2. Experimental

2.1 Materials

Acid Orange II (AO II) and PMS (Oxone®, DuPont's triple salt: $2KHSO_5•KHSO_4•K_2SO_4$) were purchased from Sigma-Aldrich Chemicals. D-glucose ($C_6H_{12}O_6•H_2O$), $Co(OAc)_2•4H_2O$, $FeCl_3•6H_2O$, $FeSO_4•7H_2O$, Co_3O_4 (30 nm), ammonium hydroxide (25%), sulfuric acid, sodium hydroxide, methanol, ethanol and *tert*-butyl alcohol (TBA) were purchased from Sinopharm Chemical Reagents Co. Ltd, China. All chemicals and reagents were of analytical grade and were used as received without further purification. All aqueous samples were prepared by using doubly distilled water (DDW).

2.2 Preparation of magnetic nanoparticles (MNPs) Fe_3O_4@C

Magnetic carbon shell nanoparticles MNPs Fe_3O_4@C were synthesized via modification of literature methods.[8, 29] $FeCl_3·6H_2O$ (5.40g, 0.02 mol), $FeSO_4·7H_2O$ (2.78g, 0.01 mol) and D-glucose (7.92g, 0.04 mol) were separately added into 50 mL of an aqueous HCl solution (pH = 1.5). The mixed solution was then added dropwise into 40 mL of an ammonia solution (3.5 mol L^{-1}) at 60°C under ultrasound irradiation. After reaction for 40 min, the mixture was transferred into a Teflon-lined autoclave (120 mL) and treated in an oven at 180 °C for 18 h. After cooling down to room temperature, the black suspension was collected by magnetic separation, washed with DDW to neutral pH, followed by washing twice with methanol. The obtained black powder was dried at 60 °C, and it was labelled as Fe_3O_4@C.

MNPs Fe_3O_4 was also prepared by unltrasonic irradiation reaction according to above procedure without addition of D-glucose and a hydrothermal treatment. The black precipitate separated after ultrasound reaction was named as MNPs Fe_3O_4, and it was used for comparison in materials characterization and the control experiments.

2.3 Preparation of Fe_3O_4@C/Co

Magnetic carbon nanospheres supported cobalt (Fe_3O_4@C/Co) was synthesized by an impregnation method followed by heat treatment.[8] A mixture containing 1.0 g of Fe_3O_4@C and 0.34 g of $Co(OAc)_2•4H_2O$ in 50 mL of ethanol was stirred for 30 min at room temperature. The temperature was increased to 50 °C to evaporate ethanol whilst stirring. The dried mixture was then calcinated in a muffle furnace at 900 °C for 1 h in nitrogen atmosphere. The sample was then washed with DDW and ethanol, respectively, followed by drying in an oven at 80 °C. The samples were denoted as Fe_3O_4@C/Co. The Co content in the Fe_3O_4@C/Co sample was determined to be 14%.

When the amount of $Co(OAc)_2•4H_2O$ was changed to 0.17 g and 0.68 g, respectively, while the

amount of Fe_3O_4@C and the preparation procedures remained unchanged, Fe_3O_4@C/Co with Co-content of 7.6% and 30%, respectively, were obtained. The samples were designated as Fe_3O_4@C/Co-7.6% and Fe_3O_4@C/Co-30%, respectively.

2.4 Characterization of materials

FT-IR spectra were recorded using an AVATAR 360 spectrometer (Nicolet, USA), and KBr pellets were used for solid samples. X-ray powder diffraction (XRD) patterns were recorded on an Empyrean diffractometer (PANalytical, B.V Company) with a Cu Kα radiation generated at 40 kV and 40 mA. A JEM-2010 transmission electron microscope (TEM) (Japanese Electronic Optical Co. Ltd., Japan) was used to obtain the information about particle size and morphology of the samples. Surface area and porous structure parameters were characterized by Brunauer-Emmett-Teller (BET) and Barrett-Joyner-Halenda (BJH) methods through N_2 adsorption and desorption at 77 K using Quantachrome Autosorb-1-C-TCD Automated Gas Sorption System (Quantachrome Instruments, USA). X-ray photoelectron spectroscopy (XPS) was recorded on a VG Multilab 2000 spectrometer (Thermo Electron Corporation) with Al Kα radiation as the exciting source (300 W). Charging effects were corrected by adjusting the binding energy of C 1s to 284.6 eV. The static magnetic properties were examined at room temperature by means of a vibrating sample magnetometer (XPMS XL-7, Quantum Design, USA). Concentration of the dye in aqueous solution was determined using a Varian Cary 50 Scan UV–Vis spectrophotometer (Varian, USA). pH measurements were made by using a Starter-3C digital pH meter (OHAUA Instrument (Shanghai) Co. Ltd, China). Cobalt content in solution was analyzed by atomic absorption spectrometer (TAS-990, Beijing Purkinje General Instrument Co. Ltd., China). Ultrasound irradiation was carried out in an ultrasound clean bath (SB-5200D, Ningbo Scientz Biotechnology Co. Ltd., China) operating at a power of 200 W.

2.5 Catalytic decolorization experiments in "Fe_3O_4@C/Co + PMS" system

Decolorization experiments were performed in a 100 mL flask at ambient temperature and under normal laboratory light. After the desired amount of organic dye in 50 mL of the aqueous solution was added into the flask, the reaction was initiated by adding Fe_3O_4@C/Co and PMS (Fe_3O_4@C/Co samples with Co-content of 14% were used unless otherwise stated). The flask was shaken on a shaker at a speed of 300 rpm. Since PMS is an acidic oxidant, the addition of PMS led to a significant decrease of pH, and the experiment was conducted at acidic medium (pH 4.05, no adjustment).[30] For studying the effect of initial

solution pH on the decolorization of AO II, H_2SO_4 (20 mM) and NaOH (20 mM) were used to adjust the solution pH after acidic salt PMS was added into the solution. For the catalyst recycling experiment, the catalyst was separated by external magnetic field and washed twice with DDW after each recycle, followed by adding a fresh solution of AO II and PMS to start the next reaction. To monitor the decolorization process of AO II, solution samples were taken out at given time intervals and measured immediately on a Varian Cary 50 Scan UV-vis spectrophotometer under the maximum absorption wavelength (484 nm). All the measurements were conducted in triplicate with a mean deviation lower than 0.01 to ensure the reproducibility of the experimental results.

3. Results and discussion

3.1 Preparation of the composites

Magnetic nanocomposites Fe_3O_4@C and Fe_3O_4@C/Co were prepared by the approach as illustrated in Scheme 1 via modification of literature methods.[8, 29] Fe_3O_4 nanoparticles were prepared by ultrasonic reaction in ammonium solution using Fe^{2+} and Fe^{3+} as iron source. A thin layer of carbon was coated on the surface of the magnetite particles through the feasible carbonization of glucose under hydrothermal condition.[8, 13, 31] The functional groups on the surface of carbon shell, such as –COOH, –OH and –C=O, were a benefit to immobilize the catalytic active species.[22, 31] The metallic ions from $Co(OAc)_2$ can be adsorbed by hydrophilic groups on the surface to Fe_3O_4@C in ethanol, followed by reduction by carbon or other reducing agents formed in-situ during the calcination process at 900 ^oC under nitrogen, generating Co^0 nanoparticles loaded Fe_3O_4@C composites, Fe_3O_4@C/Co.

The characterization of XRD and magnetic property in later part confirmed that zero valence cobalt (Co^0) was the main species deposited on the carbon shell upon the calcination. The proposed formation of mainly Co^0 rather than cobalt oxides (Co_xO_y) during calcination at 900 ^oC under nitrogen may be attributed to the fact that the organic ligands in the carbon shell were decomposed at high temperature into carbon and different kinds of gases including hydrogen, carbon monoxide, together with other fragments, which have strong reducibility and thus the cobalt ions or cobalt oxides were reduced to Co^0 metal particles.[27, 31] However, as reported by Wang *et al*, Co_3O_4 loaded Fe_3O_4@C/Co_3O_4 nanoparticles were obtained by calcining Fe_3O_4@C and Co^{2+} in air atmosphere.[8] Similarly, Zhang *et al* found that core–shell structured magnetic Fe_3O_4@C/Cu or Fe_3O_4@CuO nanocomposites could be synthesized via direct calcination of MOF based materials of magnetic Fe_3O_4@HKUST-1 in N_2 or air atmosphere, respectively.[27] Chu *et al*

entrapped Co^{2+} (Fe^{3+}) into polyacrylonitrile (PAN) template microspheres, and pyrolysis of the template microspheres containing these metal complexes at 800 °C for 1 h under a nitrogen atmosphere produced metal nanocrystals (Co^0 or Fe^0) embedded in the carbon microsphere.[32] Gong *et al* also prepared magnetic core/shell Co@C spheres using mixed plastics (consisting of polypropylene, polyethylene and polystyrene) as carbon source and it reduced Co_3O_4 to Co^0 during the carbonization at 700 °C under nitrogen atmosphere.[25] Shi *et al* found that the valence state of cobalt oxide and the reduction degree of graphene oxide (GO) of Co_3O_4/GO composites varied according to different calcination conditions. When the temperature was increased to greater than 200 °C, Co_3O_4 was reduced to CoO by the C or CO from the carbon sources of graphene or graphite under N_2 atmosphere. When the temperature rose to about 700 °C, the reduction reaction occurred in-depth, and Co_3O_4 and CoO would be reduced to metallic Co. It is of note that the Co_3O_4/GO composites catalysts calcined at 900 °C exhibited high activity for the decolorization of Orange II with PMS.[33]

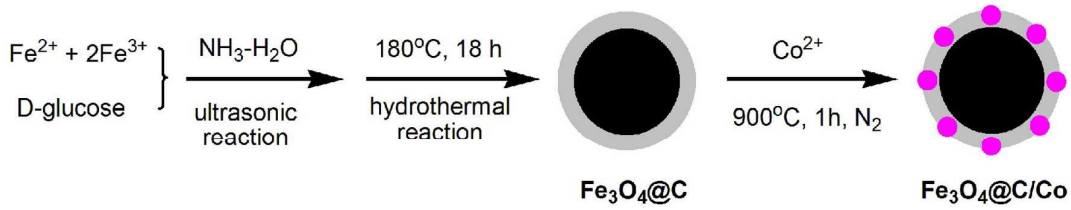

Scheme 1 Preparation procedure of Fe_3O_4@C/Co composites

3.2 Characterization of the composites

The FT-IR spectra for Fe_3O_4@C/Co and its precursors are shown in Fig. 1. The strong band at 580 cm^{-1} is a characteristic signal of the Fe–O vibrations, the peaks at 1450 cm^{-1}, 1640 and 1745 cm^{-1} are attributed to C=C, O-H, and C=O vibrations, reflecting the aromatization and carbonization of the glucose during hydrothermal treatment.[22, 34] The absorption at 3440 cm^{-1} implies the existence of residual hydroxyl groups. The peaks at 1000–1400 cm^{-1} correspond to the C–OH stretching, O–H bending and C–O–C vibrations.[8, 22] The absorptions at 2845 cm^{-1} and 2925 cm^{-1} are characteristics of aliphatic C–H stretching vibrations.[35] Fig. 1 shows that the spectrum curve of Fe_3O_4@C/Co is smoother than that of Fe_3O_4@C. As shown in Fig. 1, the peaks in the regions of 1000–1400 cm^{-1} and 2845-2950 cm^{-1} disappeared or weakened after calcination, indicating that the surface feature of Fe_3O_4@C was reconstructed after cobalt loading. Comparison of the FT-IR spectra indicated that some of the C=O and –OH functional groups in Fe_3O_4@C

were also removed during the heat treatment.[8]

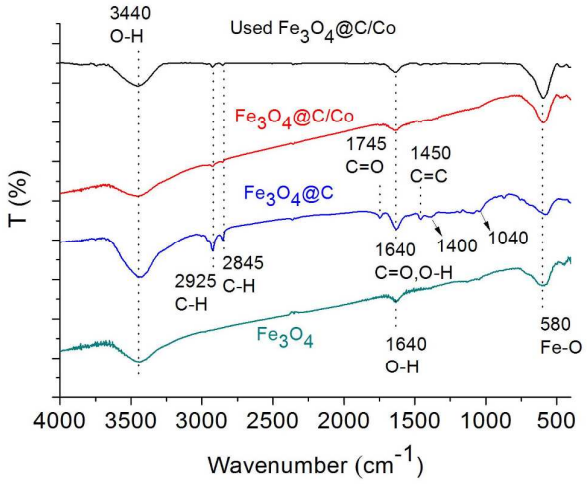

Fig. 1 FT-IR spectra of Fe_3O_4@C/Co and its precursors

X-ray powder diffraction patterns for Fe_3O_4, Fe_3O_4@C and Fe_3O_4@C/Co are shown in Fig. 2. Six characteristic peaks of Fe_3O_4 were observed at 2θ = 30.2°, 35.5°, 43.3°, 53.6°, 57.2° and 62.7°.[8, 29] The characteristic peaks for Fe_3O_4 were also observed in Fe_3O_4@C and Fe_3O_4@C/Co, suggesting that the magnetic Fe_3O_4 nanospheres were successfully encapsulated and further hydrothermal and calcination treatment did not affect the original crystallinity of Fe_3O_4 structure.[8, 13] No diffraction peaks corresponding to the graphite (2θ = 26°) are observed, indicating that most of the carbon prepared with this method was amorphous.[8, 13] XRD pattern for Fe_3O_4@C/Co shows a sharp diffraction peak of metallic cobalt (2θ = 44.5°), confirming that crystalline Co^0 nanoparticles are embedded in the carbon matrix.[35, 36] The XRD pattern for Co^0 in Fe_3O_4@C/Co corresponds to (111) diffraction of the fcc (face-centered cubic) cobalt phase.[37-39] The presence of ferromagnetic Co metal particles is also confirmed by magnetization measurements as described in later part. It should be pointed out that, although XPS measurement found Co_xO_y, no peaks associated with reflections of Co_xO_y (CoO, Co_2O_3 or Co_3O_4) were observed in the XRD diffraction.[8, 17, 36] This suggests that only a small amount of cobalt oxides are present on the surfaces of the Fe_3O_4@C/Co composite, which are formed by air passivation.[32] Nevertheless, XRD analysis confirmed that cobalt in the Fe_3O_4@C/Co composites mainly presented as zero valence Co nanoparticles with a crystalline structure, and this is in accordance with the analysis in *section 3.1*.

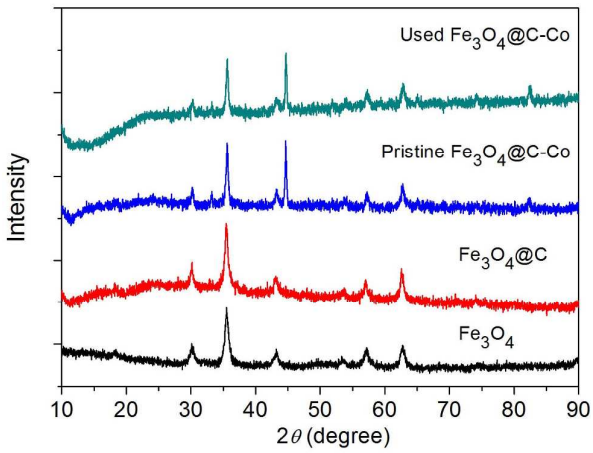

Fig. 2 XRD patterns of Fe_3O_4@C/Co and its precursors

Fig. 3 shows the room temperature magnetic hysteresis loops of the samples. All the samples exhibited typical ferromagnetic behavior. The saturation magnetization (*M*s) values for the Fe_3O_4, Fe_3O_4@C and Fe_3O_4@C/Co nanocomposites are 62.2, 37.0, and 71.7 emu/g, respectively. The *M*s value of Fe_3O_4@C is much lower than that of Fe_3O_4 nanoparticles, which is ascribed to the existence of nonmagnetic carbon in the total mass.[22] The coercivity of Fe_3O_4@C/Co is much higher than that of Fe_3O_4 and Fe_3O_4@C, and this may be caused by the enhanced shape and magnetic anisotropy in the sample of Fe_3O_4@C/Co.[40-42] It is noteworthy that the open hysteresis loops characteristics was also observed for Co^0/C core/shell sphere prepared from carbonization of mixed plastics and Co_3O_4 at 700 ^oC in N_2.[25] The *M*s of sample Fe_3O_4@C/Co is impressively high, it is higher than that of Fe_3O_4 and almost twice that of Fe_3O_4@C. It is known that cobalt itself is ferromagnetic, but its oxides (Co_3O_4 and CoO) are antiferromagnetic at room temperature.[32, 35, 41] Therefore, the high *M*s of Fe_3O_4@C/Co strongly supports that the loaded cobalt was mainly metallic Co^0 as also proved by the XRD characterization. Only a small amount of antiferromagnetic cobalt oxide may present on the surface of the nanocomposites (from XPS result in later part), and the bulk carbon matrix prevents ferromagnetic cobalt from oxidation, which makes the final products air-stable.[32]

The higher *M*s ensured better magnetic response of the magnetic nanocomposites towards an external magnetic field. The magnetic separability of Fe_3O_4@C/Co nanocomposites was tested in water by placing a magnet near the glass bottle. It was found that the samples were completely attracted to a magnet within a very short time and the solution became clear and transparent (inset in Fig. 3), confirming convenient separation of the Fe_3O_4@C/Co nanocomposites from liquids by using an external magnetic field.

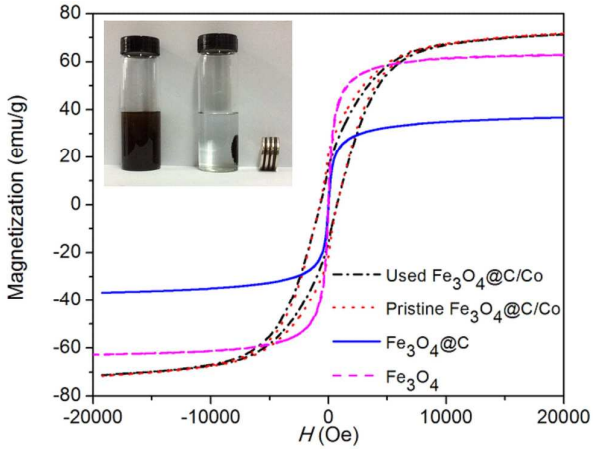

Fig. 3 Magnetization curves measured at room temperature for Fe_3O_4@C/Co and its precursors (inset showing magnetic separation of Fe_3O_4@C/Co)

TEM was applied to reveal the dimension and surface morphology of the as-prepared samples. Fig. 4a shows that the nanoparticles of Fe_3O_4 are generally homogeneous and spherical with the diameters mainly ranging from 10 to 15 nm. After carbonization, the TEM image of the obtained products Fe_3O_4@C (Fig. 4b) shows core-shell structures with an amorphous grey carbon coating layer on the surface. TEM of Fe_3O_4@C particles showed high aggregation which could be assigned to the inter-molecular magnetic dipolar interaction [8] and the self-interaction of the surrounding layer of hydrophilic polar groups. [43] Compared with Fe_3O_4, the size of many Fe_3O_4@C particles was vividly increased due to the agglomeration of Fe_3O_4 inside the nanospheres and surface growth of carbon on the shell. Fig. 4(c) shows that Fe_3O_4@C can maintain their roughly spherical shapes after calcination of the Co^{2+}-impregnated composites at 900 ^oC under N_2 forming Fe_3O_4@C/Co, but the Fe_3O_4@C/Co particles were also agglomerated and irregular carbon surfaces were observed. The cobalt nanoparticles cannot be observed directly because of the low contrast between the Co nanoparticles and the carbon matrix.[32] The surface of Fe_3O_4@C/Co is not smooth and it may be due to the aggregation of Co crystals. [35]

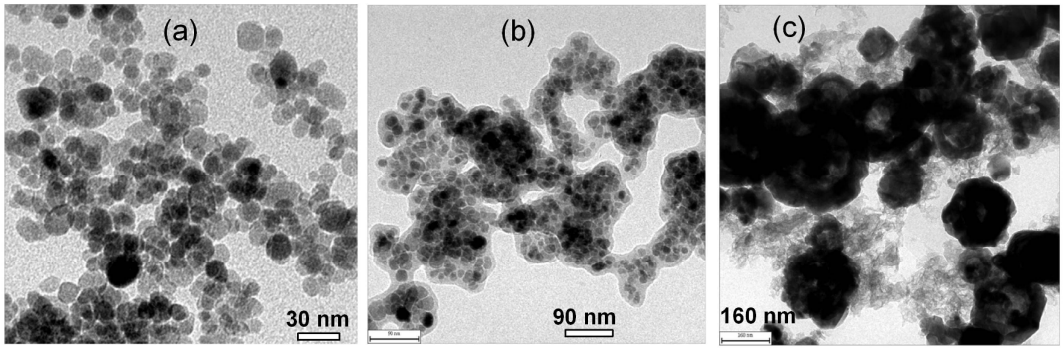

Fig. 4 TEM images of nanoparticles (a) Fe_3O_4, (b) Fe_3O_4@C, and (c) Fe_3O_4@C/Co

The specific surface area and pore volume of the samples were determined using the nitrogen sorption technique, with typical isotherms shown in Fig. 5 and the corresponding parameters of porous structure listed in Table 1. The surface area of Fe_3O_4@C/Co is much higher than that of Fe_3O_4@C while the pore volume and pore size of Fe_3O_4@C/Co are smaller than those of Fe_3O_4@C. The isotherms can be ascribed to type IV with a distinct hysteresis loop, indicating the mesoporous structures of Fe_3O_4@C and Fe_3O_4@C/Co samples.[8, 42] Fig. 5 shows that Fe_3O_4@C/Co has a narrower pore size distribution than Fe_3O_4@C and this may be ascribed to that calcination can regulate the pore size by desorption of organic substances from the carbonaceous matter and partial oxidation of carbon.[8]

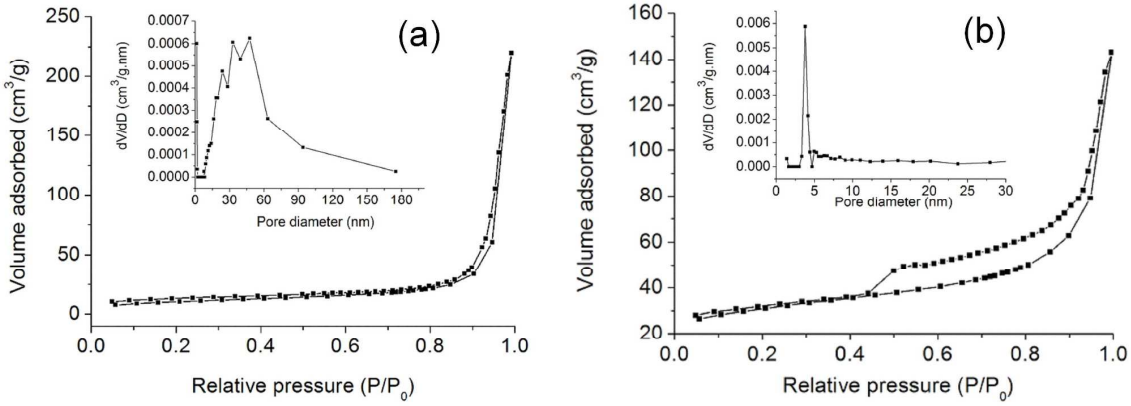

Fig. 5 Nitrogen adsorption–desorption isotherm and the corresponding pore size distribution (inset) of (a) Fe_3O_4@C, and (b) Fe_3O_4@C/Co.

Table 1 Parameters of porous structure of the samples

Sample	BET surface area (m^2 g^{-1})	Pores volume (cm^3 g^{-1})	Average pore diameter (nm)
Fe_3O_4@C	35.6	0.34	38
Fe_3O_4@C/Co	96.9	0.22	9

XPS measurement was applied to investigate the oxidation states and surface chemical compositions of Fe_3O_4@C/Co composites and the results are shown in Fig. 6. The wide survey spectrum shows that the sample consists of carbon, oxygen, iron and cobalt.[44] The spectrum of Co 2p is shown in Fig.6 (b). Gaussian–Lorentzian curve fitting of Co 2p3/2 and Co 2p1/2 was performed to describe the oxidation states. The typical Co 2p 3/2 and Co 2p 1/2 at 780.7 eV and 796.4 eV of cobalt oxides (Co_xO_y) are found. The satellite peaks at 786.0 eV and 803.0 eV are characteristic of the Co^{2+} and Co^{3+} phase.[32, 33, 36] The appearance of cobalt oxides in the surface layer can further be verified by inspecting the O 1s spectrum (Fig.5 c). A peak located at 529.8 eV is found, which is related to the binding energy of the cobalt oxides.[32] The absence of any peak at 778 eV suggested the absence of metallic Co 2p3/2.[45] XPS spectra of the metallic cobalt anchored graphene composites, Co-graphene, prepared separately by Yao *et al* [28] and Chen *et al* [46] via different approaches also indicated that the surface cobalt was present as cobalt oxide since the cobalt on the surface of graphene sheet was easily oxidized due to the small particle size and high surface area.[28, 46] It is worthy of noting that due to the limited penetration depth of XPS (< about 10 nm), XPS data reflect only the surface information of the hybrid materials, which inflated the contribution of Co_xO_y on the surface of Fe_3O_4@C/Co products. However, according to XRD measurements, there are no peaks associated with the reflections of Co_xO_y. Based on the results of XRD and magnetic measurement, it is rational to assume that only a very small amount of cobalt oxides is present on the surfaces of the Fe_3O_4@C/Co composite, which are formed by air passivation (XPS results). The carbon matrix prevents metallic cobalt nanoparticles inside the bulk Fe_3O_4@C/Co samples from oxidation, making the final products air-stable.[32]

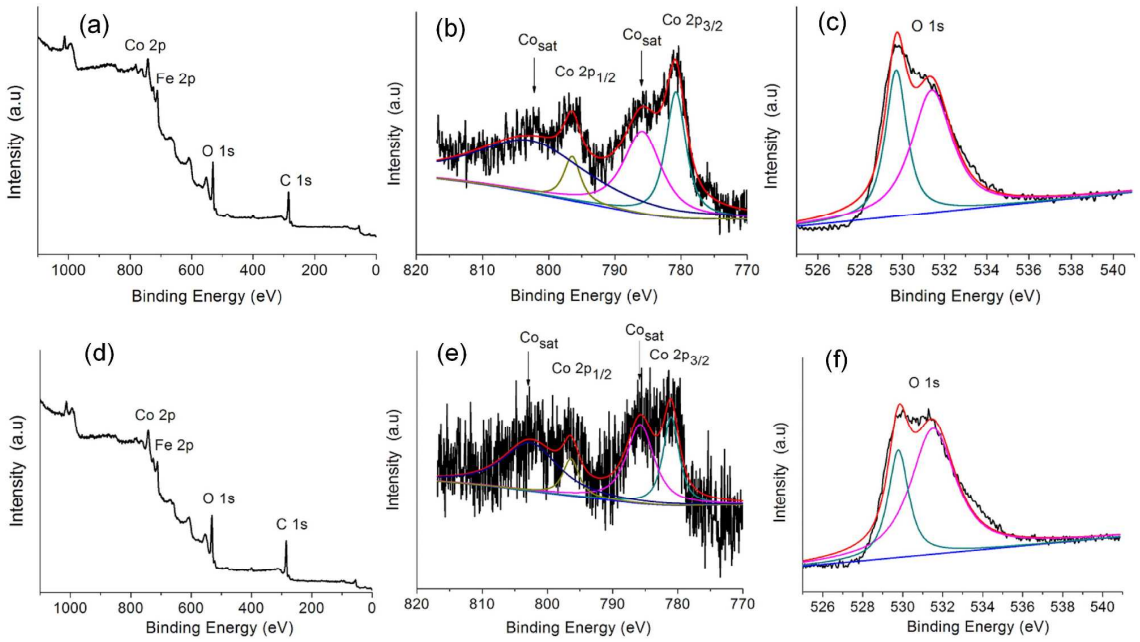

Fig. 6 X-ray photoelectron spectroscopy of Fe_3O_4@C/Co nanocomposites: (a), (d) survey spectrum; (b), (e) Co 2p peak; (c), (f) O 1s peak. (a)-(c) for pristine samples, (d)-(f) for recycled samples.

3.3 Catalytic activity of "Fe_3O_4@C/Co + PMS" system

The catalytic performances of different samples and composites are shown in Fig. 7. It can be seen that Fe_3O_4@C/Co displayed high efficiency for AO II decolorization with a removal of 99% after 40 min in the presence of PMS, while the removal rate was about 2% using only PMS, indicating that PMS could not degrade the azo dye directly and not be activated by daylight irradiation. For the experiment with sole Fe_3O_4@C, only 25% of AO II was removed in 40 min while about 50% removal of AO II was achieved in 2 hours, probably due to the adsorption ability of Fe_3O_4@C. [11, 47] For the experiment with only Fe_3O_4@C/Co, 16% of AO II was removed in 2 hours. Table 1 shows that Fe_3O_4@C/Co sample possesses higher surface area and lower pore volume than Fe_3O_4@C, therefore, we may assume that the lower removal ability of Fe_3O_4@C/Co compared with Fe_3O_4@C may due to the supported cobalt which occupies the specific surface and pore volume on the nanocomposites. On the other hand, compared with Fe_3O_4@C/Co, Fe_3O_4@C has more groups such as –OH and C=O on the surface of the carbon shell, and they might also contribute to the increased adsorption via hydrogen bond interaction with AO II. The results in Fig. 7 show that the adsorption of Fe_3O_4 and Co_3O_4 for AO II was very small while both Fe_3O_4 and Co_3O_4 can activate PMS for the decolorization of AO II. About 80% and 30% of AO II was removed in 2 h, respectively, when

Co_3O_4 and Fe_3O_4, respectively, were used as catalyst for PMS activation. The catalytic efficiency of Co_3O_4 was much higher than that of Fe_3O_4.[48] It was also reported that Fe_3O_4 exhibited minor activity for PMS activation in degradation of phenol.[13] It has been reported that activated carbon could activate PMS to degrade azo dye Acid Orange 7 in aqueous solution.[49, 50] In our work, it was found that 55% of AO II was removed in 40 min and about 85% of AO II could be degraded in 2 hour by using Fe_3O_4@C to activate PMS. This suggests that carbon on the Fe_3O_4@C plays more role than Fe_3O_4 in activating PMS, and this is due to that carbon is an electron catalyst and contains functional groups that can activate PMS producing reactive SO_4^{-}• radicals.[49, 51] It was seen that the AO II decolorization rate using different catalysts under the same operation decreased in the order: Fe_3O_4@C/Co > Fe_3O_4@C > Co_3O_4 > Fe_3O_4. Therefore, the results here strongly suggest that the loaded Co species in Fe_3O_4@C/Co has a specific function in making Fe_3O_4@C/Co as a highly efficient catalyst for activating PMS to produce more reactive SO_4^{-}• and/or HO• radicals, resulting in high removal rate of AO II in aqueous solution. These results clearly indicated that Fe_3O_4@C/Co + PSM system is an efficient catalytic system for remediation of dyes wastewater.

For the "Fe_3O_4@C/Co + PSM" system, the concentration of Co in the reaction solution was detected to be 0.08 mg/L, which was contributed to the leached Co from Fe_3O_4@C/Co. As a comparison, homogeneous catalysis by Co (II) ion (with a concentration of 0.08 mg/L) was further investigated in the same reaction system, as shown in Fig. 7. Compared to the activity of Fe_3O_4@C/Co catalysts, Co leaching has a minor contribution to the activity in PMS activation, indicating that the decolorization process is heterogeneously conducted on Fe_3O_4@C/Co.[11]

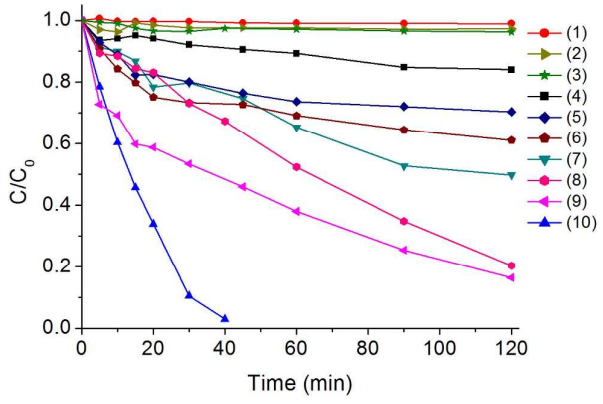

Fig. 7 Decolorization of AO II with different systems: (1) PMS; (2) Fe_3O_4; (3) Co_3O_4; (4) Fe_3O_4@C/Co; (5) Fe_3O_4 + PMS; (6) 0.08 mg/L Co(II) + PMS; (7) Fe_3O_4@C; (8) Co_3O_4 + PMS; (9) Fe_3O_4@C + PMS; (10) Fe_3O_4@C/Co + PMS. Conditions: Fe_3O_4 or Co_3O_4 or Fe_3O_4@C or Fe_3O_4@C/Co 0.2 g/L, PMS 0.1 g/L, AO

II 20 mg/L, 25°C.

In order to further ascertain the efficiency of Fe_3O_4@C/Co + PMS system for AO II decolorization, UV–Vis spectroscopy was used to identify the products during the decolorization. Representative UV–Vis spectra changes observed during the reaction are depicted in Fig. 8. For the AO II solution before reaction, it shows a main absorption bands at 484 nm, corresponding to the n–π* transition of the azo form, and another two bands at 230 and 310 nm in the ultraviolet region, which is attributed to the π–π* transition of the benzoic and naphthalene ring, respectively.[11, 30] Addition of Fe_3O_4@C/Co and PMS into the aqueous solution caused the absorption bands of the dye in the visible region to decrease with time and finally to disappear, indicating the destruction of its chromophoric structure in the vicinity of the azo-linkage. At the same time, the decrease of the two bands at 230 and 310 nm was observed, due to the opening of the benzene and naphthalene ring. [11, 30] The absorption band around 250 nm increased with the reaction time, and this may be attributed to the formation of some aromatic intermediates such as naphthalene ring (eg. 1-amino-2-naphthol) and benzene ring (eg. sulfanilamide). [5, 52]

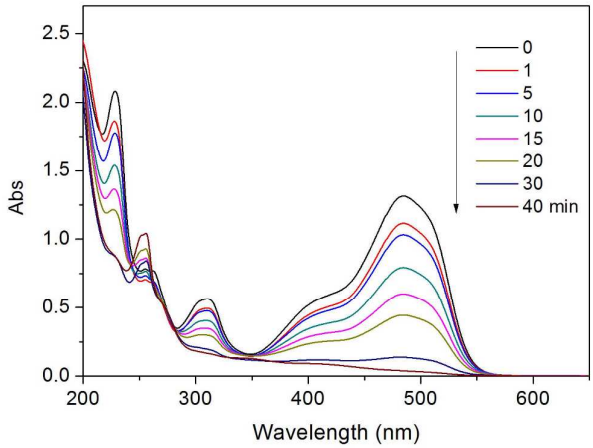

Fig. 8 Representative UV-vis spectra changes during AO II decolorization by Fe_3O_4@C/Co + PMS system. Conditions: Fe_3O_4@C/Co 0.2g/L, PMS 0.1 g/L, AO II 20 mg/L, 25°C

3.4 Effect of reaction parameters on AO II decolorization *with Fe_3O_4@C/Co + PMS system*

To further elucidate the efficiency of Fe_3O_4@C/Co + PSM system for AO II decolorization, the effect of different operating parameters, including the concentrations of Fe_3O_4@C/Co and PMS, the temperature and initial solution pH was investigated.

The influence of initial solution pH on AO II decolorization is shown in Fig. 9 (a). The dye solution

with addition of PMS had an acidic pH value of 4.05 without adjustment. For the test of pH effect, the pH value of the dye solution was adjusted with diluted H_2SO_4 and NaOH solutions. The results showed that 99% of AO II degraded in 40 min when the solution pH was not adjusted (pH = 4.05), while almost complete decolorization of AO II was achieved in 20 min when the initial solution pH was in the near neutral region (pH 6.4 – 8.5). When the initial solution pH value was decreased to 2.1 or increased to 10.9, the AO II decolorization rate became much slower. However, a removal of *ca.* 90% could still be achieved within 2 h, implying that the catalyst still exhibited a good catalytic activity.[11] When pH < 3, the metallic cobalt could be dissolved and the activation would behave the same as that of homogenous Co^{2+} ions. Excess Co^{2+} ions will react with SO_4^{-}• radicals, resulting in poor utilization of PMS. In addition, the activation at acid condition may also produce too much SO_4^{-}• radicals, which enhance radical–radical scavenger reactions.[15] Under basic conditions, SO_4^{-}• radicals can convert into HO• radicals through Eq. (3), and SO_4^{2-} is the major abundant product in the PMS oxidation system, which may play a role in scavenging HO• radicals and lead to low AO II removal efficiency.[15, 53] The results found here are consistent with the pH range (4 < pH < 9) reported for higher organic degradation efficiency by SO_4^{-}• free radicals.[4] These phenomena are also in accordance with the results reported by Liang *et al.* that a higher activity under neutral conditions was obtained when they investigated the influence of pH on persulfate oxidation of trichloroethylene at ambient temperature.[53] Thus, the high catalytic efficiency of Fe_3O_4@C/Co for activation of PMS in neutral pH range can find promising applications in the practical wastewater treatment.

$$SO_4^{-}\bullet + OH^{-} \rightarrow SO_4^{2-} + HO\bullet \quad (3)$$

The influence of Fe_3O_4@C/Co catalyst dosage on the decolorization of AO II by Fe_3O_4@C/Co + PMS system is illustrated in Fig. 9 (b). The results indicate that the decolorization of AO II was significantly influenced by the dosage of catalyst. The decolorization efficiency at 30 min was enhanced from 69% to 99% when the catalyst dosage was increased from 0.1 g L^{-1} to 0.3 g L^{-1}. This fact is evidently attributed to the increased active sites on the surface of Fe_3O_4@C/Co catalyst for reaction with PMS, which will generate more reactive radicals. In addition, the dye adsorbed on the catalyst increased with increase of Fe_3O_4@C/Co catalyst dosage, which could also enhance the decolorization rate.[8, 30, 54] The decolorization efficiency increased relatively slower when the catalyst dosage increased from 0.2 g L^{-1} to 0.3 g L^{-1}, which may be mainly attributed to possible scavenging of radicals by the reaction between excess active sites and

the sulfate and hydroxyl radicals.[54, 55]

The decolorization of AO II over Fe_3O_4@C/Co was further studied at varying PMS concentrations. As shown in Fig. 9 (c), AO II was slowly degraded in the presence of 0.05 g/L of PMS, the slow removal of AO II was probably due to lack of sufficient oxidant amount.[30, 54] When PMS concentration was increased to 0.1 g/L, the decolorization efficiency increased significantly, as more active radicals could be produced under a high concentration of PMS. [30, 54] However, further increase in PMS concentration to 0.2 g/L did not result in the same increasing trend of the decolorization efficiency. The fact may be due to that the reaction proceeds via radical mechanism, and this was possibly due to the self-quenching of sulfate and hydroxyl radicals by PMS. [8, 30]

The effect of reaction temperature on AO II decolorization is shown in Fig. 9 (d). It is seen that reaction temperature dramatically affected the decolorization efficiency of AO II. A general trend can be observed that higher temperature will result in an increase in the decolorization rate. When reaction took place at 20 ^{o}C, almost a complete AO II decolorization was achieved in *ca*. 80 min while the time would be reduced to *ca*. 40 min at 25 ^{o}C. The duration would be further reduced to 25 min when the reaction temperature was increased to 35 ^{o}C. The results revealed that the PMS activation process was an endothermic reaction, and higher temperature would drive the reaction to produce more active sulfate and hydroxyl radicals and thus enhance the AO II decolorization efficiency.[8, 54]

The effect of cobalt content in the catalyst Fe_3O_4@C/Co on AO II decolorization was also evaluated and the result is shown in Fig. 9 (e). Increase of Co-content in the catalyst would enhance the decolorization efficiency of AO II and it can be attributed to the increased active sites on the catalyst.

Variation of pH during the reaction processes was also monitored by adjusting reaction solution pH after addition of PMS, and the results are shown in Fig. 9 (f). It was found that the pH remained essentially unchanged with only a slight variation for the reaction with initial pH of 2.10 and 4.05. However, for the reaction with initial pH of 8.50, the pH decreased with the increase of reaction time. The pH decreased markedly to about 4.3 at 30 min (reaction finished according to Fig. 9 (a)) and remained unchanged for the followed reaction process. Similar phenomenon was also observed in the degradation of AO II by "$Fe_{3-x}M_xO_4$ (Cr, Mn, Co, Ni) + PMS" system [56] and "Fe-Co/SBA-15 + PMS" system. [4] When the pH was raised, OH^-/H_2O would be oxidized by SO_4^{-}• and converted into HO•, generating H^+ and consuming OH^- (Eq. (3) and (4)). On the other hand, the dissociation of HSO_4^- (Eq. (5)), which was formed as a result of the reaction between hydroxyl radical and sulfate radical (Eq. (6)), would further release H^+ and decrease

the solution pH.[4, 56]

$$SO_4^{-}\bullet + H_2O \rightarrow SO_4^{2-} + HO\bullet + H^+ \quad (4)$$

$$HSO_4^{-} \rightarrow SO_4^{2-} + H^+ \quad (5)$$

$$SO_4^{-}\bullet + HO\bullet \rightarrow HSO_4^{-} + 1/2O_2 \quad (6)$$

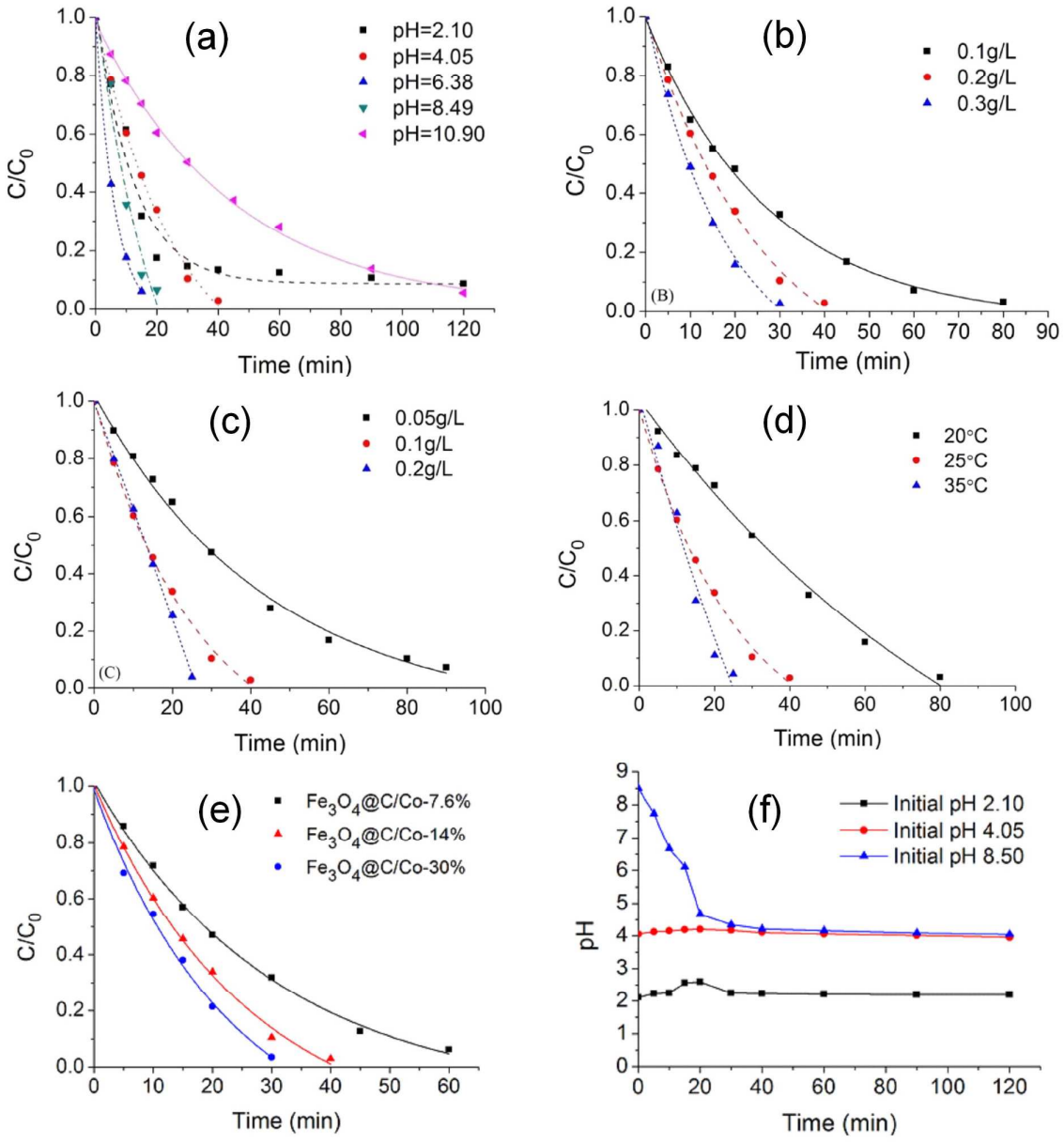

Fig. 9 Influence of initial solution pH (a), Fe_3O_4@C/Co dosages (b), PMS concentration (c), reaction temperature (d), cobalt content (%) in Fe_3O_4@C/Co (e), and pH variation during reaction process (f) on AO II decolorization with Fe_3O_4@C/Co + PMS system. Conditions: (a) Fe_3O_4@C/Co 0.2g/L, PMS 0.1 g/L, AO II 20 mg/L, 25°C; (b) PMS 0.1 g/L, AO II 20 mg/L, 25°C; (c) Fe_3O_4@C/Co 0.2g/L, AO II 20 mg/L, 25°C; (d), (e) and (f) Fe_3O_4@C/Co 0.2g/L, PMS 0.1 g/L, AO II 20 mg/L

3.5 Activation mechanism of PMS on Fe_3O_4@C/Co

It has been proven that several types of reactive radicals, such as sulfate, peroxy-sulfate and hydroxyl

radicals, could be generated by PMS under activation of transition metals. SO_4^{-}• and HO• could attack the organic molecules, but SO_5^{-}• cannot due to its low redox potential (1.1 V). To identify the dominating oxidizing species responsible for AO II decolorization in the "Fe_3O_4@C/Co + PMS" system, ethanol and *tert*-butyl alcohol (TBA) were used to perform quenching studies. Ethanol is widely used as the scavenger of SO_4^{-}• and HO•, while TBA is an effective quenching agent for HO•.[50, 54] It can been seen from Fig. 10 that the addition of 1.0 M ethanol significantly inhibited AO II decolorization, leading to a decrease in the AO II removal efficiency to 14% compared to the 98% AO II removal efficiency that occurred in 40 min without addition of ethanol. When 1.0 M TBA was added to the solution, the decolorization of AO II declined to 75% in 40 min. Thus, the inhibition of AO II decolorization caused by EtOH is much stronger than that caused by TBA, indicating that sulfate radicals, SO_4^{-}•, were the dominant active species controlling the oxidation reaction in the "Fe_3O_4@C/Co + PMS" system for decolorization of AO II.[30, 54] Results in Fig. 10 show that HO• radicals might also present, but its contribution was minor compared with SO_4^{-}• radicals.[30] Fig. 10 implies that the decolorization efficiency decreased when the AO II decolorization reaction was conducted under N_2 atmosphere, and this result suggests that oxygen (from air) is involved in the decolorization process activated by Fe_3O_4@C/Co. According to the mechanisms proposed by Shi *et al* [33] and Yao *et al* [28] for the PSM activation by cobalt-loaded graphene hybrids, the mechanism of PMS activation with Fe_3O_4@C/Co catalyst is hereby proposed. At first, metallic cobalt (Co^0) nanoparticles in Fe_3O_4@C/Co composites can release Co^{2+} at certain conditions (Eq. (7) and (8)), which was employed to activate PMS to generate SO_4^{-}• for the decolorization of AO II in water (Eq. (9)). Meanwhile, Co^0 can also activate PMS to generate SO_4^{-}• (Eq. (10)). PMS can reduce Co^{3+} to Co^{2+} and generate SO_5^{-}• (Eq. (11)). Thus, Co^{2+} exhibits redox cycling in the presence of PMS and produces SO_4^{-}•, similar to iron ions in a Fenton-like reaction.[28] The highly reactive SO_4^{-}• radicals consequently react with AO II and its intermediate products to accomplish the full degradation of organic components (Eq. (12)). The reactions are listed as follows: [5, 8, 33]

$$Fe_3O_4@C/Co^0 \rightarrow Fe_3O_4@C/Co^{2+} + 2\ e^- \quad (7)$$

$$Fe_3O_4@C/Co^0 + 0.5\ O_2 + H_2O \rightarrow Fe_3O_4@C/Co^{2+} + 2\ OH^- \quad (8)$$

$$Fe_3O_4@C/Co^{2+} + HSO_5^- \rightarrow Fe_3O_4@C/Co^{3+} + SO_4^{-}\bullet + OH^- \quad (9)$$

$$Fe_3O_4@C/Co^0 + 2HSO_5^- \rightarrow Fe_3O_4@C/Co^{2+} + 2SO_4^{-}\bullet + 2OH^- \quad (10)$$

$$Fe_3O_4@C/Co^{3+} + HSO_5^- \rightarrow Fe_3O_4@C/Co^{2+} + SO_5^{-}\bullet + H^+ \quad (11)$$

$$SO_4^{-}\bullet + \text{AO II} \rightarrow \text{intermediates} \rightarrow CO_2 + H_2O \quad (12)$$

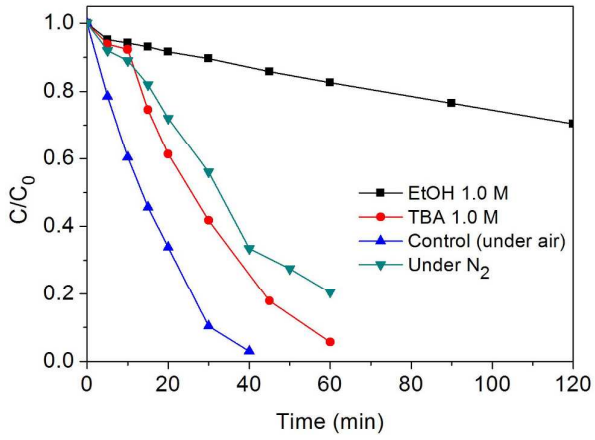

Fig. 10 Effect of EtOH, TBA and N_2 atmosphere on AO II decolorization with the Fe_3O_4@C/Co + PMS system. Conditions: Fe_3O_4@C/Co 0.2 g/L, PMS 0.1 g/L, AO II 20 mg/L, 25°C

3.6 Recycling and reusability of Fe_3O_4@C/Co catalyst

The recyclability of catalysts is an important factor for more economical processes.[22, 27] Therefore, the recyclability of catalyst Fe_3O_4@C/Co was investigated in repeated cycles of reaction. At the end of the reaction, the catalyst was separated from the reaction medium using a magnet. The catalyst was washed several times with DDW and reused for next cycle of AO II decolorization. After repeating for six times, the Fe_3O_4@C/Co composite was still stable and exhibited a high catalytic activity with the AO II decolorization efficiency of 93% in the sixth run (Fig. 11).

The separated catalyst Fe_3O_4@C/Co after the sixth reaction run was further examined by using FT-IR, XRD, vibrating sample magnetometer and XPS. Compared with the images of the pristine catalyst, FT-IR (Fig. 1), XRD (Fig. 2), Magnetization curves (Fig. 3) and XPS (Fig. 6) of the recycled catalyst did not show any obvious changes. All these analyses suggest the excellent stability and reusability of Fe_3O_4@C/Co composite. Comparison of XPS, XRD and magnetization between the pristine and recycled catalyst indicate that metallic cobalt presents in the bulk Fe_3O_4@C/Co composite and the relative content of Co^0 remains unchanged, while the surface composition of Fe_3O_4@C/Co composite was mainly cobalt oxides as observed from the XPS for the pristine Fe_3O_4@C/Co composite. Therefore, the oxidation states of the cobalt post catalysis were essentially the same as in the pristine catalyst. We may assume that the catalytic activation of PMS was performed mainly by the metallic cobalt nanoparticles inside the porous Fe_3O_4@C/Co composite.

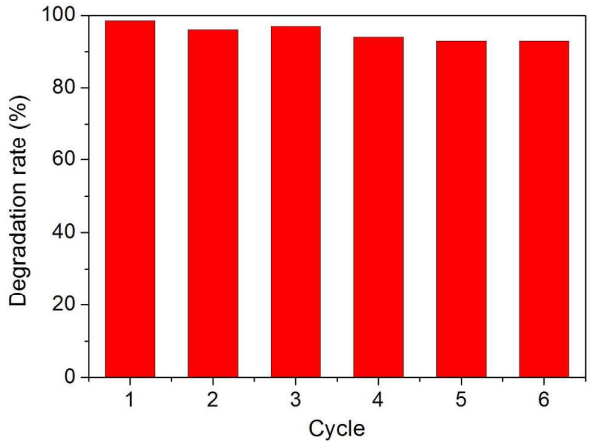

Fig. 11 The decolorization efficiency of AO II during different cycle use of Fe_3O_4@C/Co. Conditions: Fe_3O_4@C/Co 0.2 g/L, PMS 0.1 g/L, AO II 20 mg/L, 25°C, reaction time 40 min

In recent years, dye degradation has been studied using metal or metal oxide nanoparticles supported on carbon and/or graphene. A preliminary and brief comparison of oxidation removal of AO II by PMS activated with different heterogeneous cobalt catalysts is given in Table 2. A few examples of degradation of methylene blue (MB) dye and H_2O_2 or peroxydisulfate (PS) as oxidant are also included in Table 2 for comparison. It can be seen from Table 2 that the performance of Fe_3O_4@C/Co is comparable to the other materials and it also exhibits some other advantages. Therefore, the nanocomposite catalyst Fe_3O_4@C/Co might be one of the promising and feasible materials for oxidation removal of organic pollutants.

Table 2 Comparison of some heterogeneous cobalt catalysts for oxidation removal of dyes with PMS

Catalyst	Dye	Reaction conditions	Time used for > 99% removal	Advantages (A)/ disadvantages (D)	Ref.
Fe_3O_4@C/Co^0	AO II	AO II 20 mg/L, Catalyst loading 0.2 g/L, PMS/AO II = 5	40 min (pH_0 = 4) 20 min (pH_0 6.4)	**A**: Feasible preparation, high efficiency, magnetic separation, slight Co leaching **D**: relatively higher catalyst loading	This work
Co^0-graphene	AO II	AO II 60 mg/L, Catalyst loading 0.01g/L, PMS/AO II = 3.3, pH_0 = 7	30 min	**A**: small catalyst loading, high efficiency, magnetic separation, slight Co leaching **D**: relatively expensive	[28]
Co_3O_4/graphene oxide	AO II	AO II 70 mg/L, Catalyst loading 0.1 g/L, PMS/AO II = 17.4, pH_0 = 7	6 min	**A**: high efficiency, slight Co leaching **D**: relatively expensive, separation relatively difficult, higher PMS amount	[33, 57]
Mn_3O_4-rGO	AO II	AO II 30 mg/L, Catalyst loading 0.05 g/L, PMS/AO II = 50, pH_0 = 7	120 min (64% at pH 4)	**A**: small catalyst loading, **D**: higher PMS amount, longer reaction time, relatively expensive	[58]
$ZnFe_2O_4$-rGO	AO II	AO II 20 mg/L, Catalyst loading 0.1 g/L, PMS/AO II = 25, pH_0 = 7	150 min	**A**: Magnetic separation, effective under various salt **D**: lower efficiency, higher PMS amount, light irradiation required	[59]
$MnFe_2O_4$-rGO hybrid	AO II	AO II 20 mg/L, Catalyst loading 0.05 g/L, PMS/AO II = 25	120 min	**A**: Magnetic separation, small catalyst loading, small leaching of metal **D**: longer reaction time, high PMS amount	[60]
$ZnFe_2O_4$–C_3N_4 hybrid	AO II	AO II 10 mg/L, Catalyst loading 0.5 g/L, H_2O_2 0.1 M, pH_0 = 7	240 min	**A**: Magnetic separation, feasible preparation **D**: lower efficiency, high catalyst loading, light irradiation required	[61]
Fe-Co/GAC (granular activated carbon)	AO II	AO II 50 mg/L, Catalyst loading 0.8 g/L, PS/AO II = 10, pH_0 = 5.8	60 min	**A**: feasible preparation **D**: high catalyst loading, leaching for Co 6.28% (while Fe 0.76%), ultrasound assistance	[62]
$CuFe_2O_4$/activated carbon	MB	MB 20 mg/L, Catalyst loading 0.2 g/L, PMS/MB = 100, pH_0 = 5	60 min	**A**: Magnetic separation, feasible preparation **D**: higher PMS amount, relatively high catalyst loading	[51]
Fe_3O_4/Mn_3O_4/rGO	MB	MB 50 mg/L, Catalyst loading 0.1 g/L, PMS/MB = 6, pH_0 = 7	30 min	**A**: Magnetic separation, high efficiency **D**: complicated preparation, relatively expensive	[54]

4. Conclusions

Metallic Co loaded magnetic nanocomposite Fe_3O_4@C/Co were effectively synthesized from the precursor of Fe_3O_4@C impregnated with Co^{2+} through in-situ reduction of Co^{2+} to Co^0 during the high temperature calcination process under nitrogen atmosphere. The nanocomposites were characterized and Fe_3O_4@C/Co exhibited high performance in activating PMS for decolorization of AO II dye in aqueous solution. The dye solution could be completely decolorized in 40 min within a wide pH range (pH 4.1–8.5). Increase of catalyst load, PMS concentration and reaction temperature promoted the dye decolorization efficiency. The quenching studies confirmed that sulfate radicals were the primary species produced during the catalytic decomposition of PMS. Fe_3O_4@C/Co nanocomposites also exhibited good stability and reusability for 6 cycles use without deterioration in its performance. This study provides a feasible approach for removal of organic pollutants by magnetically separable catalyst. Current work is continuing in our laboratory to investigate the applications of the catalyst for the treatment of complex wastewater containing organic contaminants.

Acknowledgements

We are very grateful to the reviewers for their comments and suggestions. This work was financially supported by the National Natural Science Foundation of China (Grant No. 21277106 and 21101122); Collaborative Innovation Plan of Hubei Province for Key Technology of Eco-Ramie Industry (2014-8); Scientific and Technological Innovation Plan of Wuhan Textile University (Grant No.153031).

References

1. M. T. Yagub, T. K. Sen, S. Afroze and H. M. Ang, *Adv. Colloid. Interfac.*, 2014, **209**, 172.
2. H. Lin, H. Zhang, X. Wang, L. Wang and J. Wu, *Sep. Purif. Technol.*, 2014, **122**, 533.
3. X. Chen, W. Wang, H. Xiao, C. Hong, F. Zhu, Y. Yao and Z. Xue, *Chem. Eng. J.*, 2012, **193-194**, 290.
4. C. Cai, H. Zhang, X. Zhong and L. Hou, *J. Hazard. Mater.*, 2015, **283**, 70.
5. X. Wang, L. Wang, J. Li, J. Qiu, C. Cai and H. Zhang, *Sep. Purif. Technol.*, 2014, **122**, 41.
6. K. Singh and S. Arora, *Crit. Rev. Environ. Sci. Technol.*, 2011, **41**, 807.
7. R. Ganesh, G. D. Boardman and D. Michelsen, *Water Res.*, 1994, **28**, 1367.
8. Y. Wang, H. Sun, H. M. Ang, M. O. Tadé and S. Wang, *Chem. Eng. J.*, 2014, **245**, 1.

9. A. Rastogi, S. R. Al-Abed and D. D. Dionysiou, *Appl. Catal. B: Environ.*, 2009, **85**, 171.
10. J. Sharma, I. M. Mishra, D. D. Dionysiou and V. Kumar, *Chem. Eng. J.*, 2015, **276**, 193.
11. L. Duan, B. Sun, M. Wei, S. Luo, F. Pan, A. Xu and X. Li, *J. Hazard. Mater.*, 2015, **285**, 356.
12. Y. Tao, Q. Ni, M. Wei, D. Xia, X. Li and A. Xu, *RSC Adv.*, 2015, **5**, 44128.
13. Y. Wang, H. Sun, H. M. Ang, M. O. Tadé and S. Wang, *J. Colloid. Interf. Sci.*, 2014, **433**, 68.
14. G. Chen, X. Si, J. Yu, H. Bai and X. Zhang, *Appl. Surf. Sci.*, 2015, **330**, 191.
15. J. Yan, L. Zhu, Z. Luo, Y. Huang, H. Tang and M. Chen, *Sep. Purif. Technol.*, 2013, **106**, 8.
16. Q. Yang, H. Choi, Y. Chen and D. D. Dionysiou, *Appl. Catal. B: Environ.*, 2008, **77**, 300.
17. G. Zhou, H. Sun, S. Wang, H. M. Ang and M. O. Tadé, *Sep. Purif. Technol.*, 2011, **80**, 626.
18. Q. Yang, H. Choi, S. R. Al-Abed and D. D. Dionysiou, *Appl. Catal. B: Environ.*, 2009, **88**, 462.
19. M. Stoyanova, I. Slavova, S. Christoskova and V. Ivanova, *Appl. Catal. A: Gen.*, 2014, **476**, 121.
20. P. R. Shukla, S. Wang, H. Sun, H. M. Ang and M. Tadé, *Appl. Catal. B: Environ.*, 2010, **100**, 529.
21. P. Shukla, S. Wang, K. Singh, H. M. Ang and M. O. Tadé, *Appl. Catal. B: Environ.*, 2010, **99**, 163.
22. W. H. Li, X. P. Yue, C.S. Guo, J.P. Lv, S.S. Liu, Y. Zhang and J. Xu, *Appl. Surf. Sci.*, 2015, **335**, 23.
23. S. H. Joo, S. J. Choi, I. Oh, J. Kwak, Z. Liu, O. Terasaki and R. Ryoo, *Nature*, 2001, **412**, 169.
24. G. Liu, F. He, J. Zhang, L. Li, F. Li, L. Chen and Y. Huang, *Appl. Catal. B: Environ.*, 2014, **150-151**, 515.
25. J. Gong, J. Liu, X. C. Chen, Z. Jiang, X. Wen, E. Mijowska and T. Tang, *J. Mater. Chem. A*, 2014, **2**, 7461.
26. S. Linley, T. Leshuk and F. X. Gu, *Clean-Soil, Air, Water*, 2013, **41**, 1152.
27. Y. F. Zhang, L. G. Qiu, Y. P. Yuan, Y. J. Zhu, X. Jiang and J. D. Xiao, *Appl. Catal. B: Environ.*, 2014, **144**, 863.
28. Y. Yao, C. Xu, J. Qin, F. Wei, M. Rao and S. Wang, *Ind. Eng. Chem. Res.*, 2013, **52**, 17341.
29. N. Wang, L. Zhu, D. Wang, M. Wang, Z. Lin and H. Tang, *Ultrason. Sonochem.,* 2010, **17**, 526.
30. S. Luo, L. Duan, B. Sun, M. Wei, X. Li and A. Xu, *Appl. Catal. B: Environ.*, 2015, **164**, 92.
31. G. Yu, B. Sun, Y. Pei, S. Xie, S. Yan, M. Qiao, K. Fan, X. Zhang and B. Zong, *J. Am. Chem. Soc.*, 2010, **132**, 935.
32. Y. Chu, P. Zhang, J. Hu, W. Yang and C. Wang, *J. Phys. Chem. C*, 2009, **113**, 4047.
33. P. Shi, X. Wang, X. Zhou, Y. Min, J. Fan and W. Yao, *RSC Adv.*, 2015, **5**, 34125.
34. X. Sun and Y. Li, *Angew. Chem. Int. Edit.*, 2004, **43**, 597.

35. R. Qiao, X. L. Zhang, R. Qiu, Y. Li and Y. S. Kang, *J. Phys. Chem. C*, 2007, **111**, 2426.

36. D. Banerjee, R. V. Jagadeesh, K. Junge, M.-M. Pohl, J. Radnik, A. Brückner and M. Beller, *Angew. Chem. Int. Edit.*, 2014, **53**, 4359.

37. Z. J. Liu, Z. Y. Yuan, W. Zhou, L. M. Peng and Z. Xu, *Phys. Chem. Chem. Phys.*, 2001, **3**, 2518.

38. J. A. Díaz, M. Martínez-Fernández, A. Romero and J. L. Valverde, *Fuell*, 2013, **111**, 422.

39. K. Maaz, S. Karim, M. Usman, A. Mumtaz, J. Liu, J. L. Duan and M. Maqbool, *Nanoscale Res. Lett.*, 2010, **5**, 1111.

40. T. N. Narayanan, M. M. Shaijumon, P. M. Ajayan and M. R. Anantharaman, *Nanoscale Res. Lett.*, 2010, **5**, 164.

41. L. Duan, S. Jia, R. Cheng and L. Zhao, *Chem. Eng. J*, 2011, **173**, 233.

42. C. He, S. Qiu, X. Wang, J. Liu, L. Luan, W. Liu, M. Itoh and K. I. Machida, *J. Mater. Chem.*, 2012, **22**, 22160.

43. T. Poursaberi and M. Hassanisadi, *Clean-Soil, Air, Water*, 2013, **41**, 1208.

44. L. Fu, Z. Liu, Y. Liu, B. Han, P. Hu, L. Cao and D. Zhu, *Adv. Mater.*, 2005, **17**, 217.

45. T. Preethi, B. Abarna, K. N. Vidhya and G. R. Rajarajeswari, *Ceram. Int.*, 2014, **40**, 13159.

46. Y. Chen, Q. Wang, C. Zhu, P. Gao, Q. Ouyang, T. Wang, Y. Ma and C. Sun, *J. Mater. Chem.*, 2012, **22**, 5924.

47. Z. Zhang and J. Kong, *J. Hazard. Mater.*, 2011, **193**, 325.

48. H. Sun, G. Zhou, S. Liu, H. M. Ang, M. O. Tadé and S. Wang, *ACS Appl. Mater. Interfaces*, 2012, **4**, 6235.

49. J. Zhang, X. Shao, C. Shi and S. Yang, *Chem. Eng. J.*, 2013, **232**, 259.

50. S. Yang, T. Xiao, J. Zhang, Y. Chen and l. Li, *Sep. Purif. Technol.*, 2015, **143**, 19.

51. W. D. Oh, S. K. Lua, Z. Dong and T. T. Lim, *J. Hazard. Mater.*, 2015, **284**, 1.

52. G. Quan, W. Sun, J. Yan and Y. Lan, *Water Air Soil Pollut.*, 2014, **225**, 2195.

53. C. J. Liang, Z. S. Wang and C. J. Bruell, *Chemosphere*, 2007, **66**, 106.

54. B. Yang, Z. Tian, B. Wang, Z. Sun, L. Zhang, Y. Guo, H. Li and S. Yan, *RSC Adv.*, 2015, **5**, 20674.

55. T. D. Nguyen, N. H. Phan, M. H. Do and K. T. Ngo, *J. Hazard. Mater.*, 2011, **185**, 653.

56. G. Wei, X. Liang, Z. He, Y. Liao, Z. Xie, P. Liu, S. Ji, H. He, D. Li and J. Zhang, *J. Mol. Catal. A: Chem.*, 2015, **398**, 86.

57. P. Shi, X. Dai, H. Zheng, D. Li, W. Yao and C. Hu, *Chem. Eng. J.*, 2014, **240**, 264.

58. Y. Yao, C. Xu, S. Yu, D. Zhang and S. Wang, *Ind. Eng. Chem. Res.*, 2013, **52**, 3637.

59. Y. Yao, J. Qin, Y. Cai, F. Wei, F. Lu and S. Wang, *Environ. Sci. Pollut. Res.*, 2014, **21**, 7296.

60. Y. Yao, Y. Cai, F. Lu, F. Wei, X. Wang and S. Wang, *J. Hazard. Mater.*, 2014, **270**, 61.

61. Y. Yao, Y. Cai, F. Lu, J. Qin, F. Wei, C. Xu and S. Wang, *Ind. Eng. Chem. Res.*, 2014, **53**, 17294.

62. C. Cai, L. Wang, H. Gao, L. Hou and H. Zhang, *J. Environ. Sci.*, 2014, **26**, 1267.

Table of contents entry:

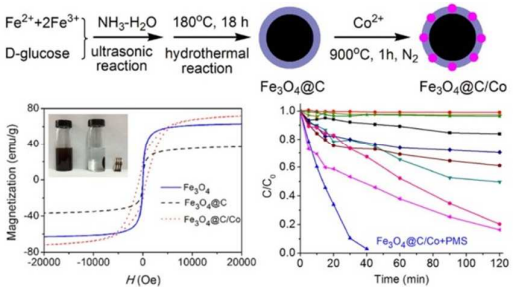

Magnetic Fe_3O_4@C/Co nanocomposites exhibited high efficiency and reusability in activation of PMS for decolorization of AO II solution.